Cement and Concrete Research 175 (2024) 107357

Contents lists available at ScienceDirect

Cement and Concrete Research

journal homepage: www.elsevier.com/locate/cemconres

Role of magnesium acetate in hydration and carbonation of magnesium oxide-based cements

Nirrupama Kamala Ilango [a], Hoang Nguyen [a,b], Alexander German [b,c], Frank Winnefeld [b], Paivo Kinnunen [a,*]

[a] Fibre and Particle Engineering Research Unit, University of Oulu, Pentti Kaiteran katu 1, 90014 Oulu, Finland
[b] Swiss Federal Laboratories for Materials Science and Technology (Empa), Laboratory for Concrete & Asphalt, Überlandstrasse 129, 8600 Dübendorf, Switzerland
[c] ETH Zurich, Institute for Building Materials, 8093 Zurich, Switzerland

ARTICLE INFO

Keywords:
Brucite
MgO cement
Mg-acetate
Carbonation
$Mg(OH)_2$

ABSTRACT

MgO-based cements have the potential for low carbon binders especially when MgO is sourced from non-carbonate minerals. Understanding the reaction kinetics and products formed are the keys to pave the way for these binders as construction materials. In this study, the influence of acetate on hydration and subsequent carbonation of reactive MgO is investigated. MgO hydrated in Mg-acetate solution of various concentrations (0 to 0.5 M) and CO_2 cured afterward was characterized at different reaction times. Magnesium acetate in addition to enhancing the hydration kinetics modifies the morphology and crystallinity of the precipitated brucite. Acetate also influences the carbonate phases formed when samples are cured with CO_2. Giorgiosite, a lesser-known hydrated magnesium carbonate, was formed in the presence of acetate, while the control specimens prepared with neat water produced nesquehonite. The findings reported here give insights into the use of organic additives in improving the reaction kinetics of MgO and the possibility to tune the formation pathways of different magnesium carbonates.

1. Introduction

Portland cement (PC) is the largest produced material on earth and the most used material globally only next to water [1]. The annual global cement production was estimated to be 4.4 billion tonnes in 2020 [2]. In the foreseeable future, an increased demand in the production of cement due to the rise in population and infrastructure development trends is assumed [3]. Although cement production is a highly energy-efficient process, it accounts for about 8 % of anthropogenic CO_2 emissions. About 60 % of the emissions result from the fossil CO_2 in calcite and the rest is mainly due to the burning of fuels to heat the kiln to 1450 °C to produce the clinker [4]. A great emphasis has been made to minimize the impact of cement production on climate by substituting clinker with different industrial side streams such as blast furnace slag (BFS), fly ash (FA), calcined clay and various other materials [5,6] referred to as supplementary cementitious materials (SCMs). Although SCMs have been the primary pathway for reducing clinker production, there has been increased interest in alternative binders such as alkali-activated cements, belite-rich cements, calcium sulfoaluminate cements, and MgO-based cements [3,7–9]. MgO-based binders are promising since they can be based on zero-carbon feedstocks and have a large potential for CO_2 emission reduction or even carbon storage [3,10].

The main precursor for magnesium-based cements has been MgO, often calcined from magnesite ($MgCO_3$) at 600 °C to 1200 °C. However, this extraction route yields an intensive CO_2 emission (1.55 kg CO_2 per kg MgO produced) [7], and hence should not be a source of MgO in producing this binder. In addition, the reactivity of MgO produced depends largely on the calcination temperature and residence time [11–13]. Other notable sources of MgO are seawater, brine solutions and magnesium silicate minerals. Producing MgO from seawater or brine solutions is also an energy extensive process [14]. Recently MgO produced from magnesium silicate minerals has gained interest due to advances in separation technologies becoming economically more feasible [15–17]. There have been works demonstrating viable routes for low-carbon Mg extraction from olivine [15] through acid digestion and electrolysis and serpentinite minerals [17] by using recoverable ammonium sulphate salts. Although cements based on magnesium

* Corresponding author.
E-mail address: paivo.kinnunen@oulu.fi (P. Kinnunen).

https://doi.org/10.1016/j.cemconres.2023.107357
Received 27 April 2023; Received in revised form 8 September 2023; Accepted 23 October 2023
Available online 4 November 2023

carbonates can theoretically reach negative carbon footprint, there is not yet a holistic assessment available for the total energy consumption and carbon footprint of these technologies. Therefore, efforts are needed to assess the techno-economic viability of such technologies and compare them to conventional Portland cement processing.

Brucite ($Mg(OH)_2$), the hydration product of MgO, has no or low mechanical strength. However, carbon curing of MgO-based binders has shown to improve the strength of binders [18]. The increase in performance is attributed to the morphology of the carbonates formed, the reduction in porosity, and the binding strength of the products formed. On carbonation, brucite reacts with CO_2 to form various hydrated magnesium carbonates (HMCs). The primary challenge in using MgO as the binder is its low reaction rate primarily due to the formation of a passivation layer consisting of $Mg(OH)_2(s)$ on the surface of MgO. Magnesium oxide hydrates to form brucite through a dissolution-precipitation process. The surface of magnesium oxide is hydroxylated in the presence of water. The OH^- ions are adsorbed on the positively charged surface and are in equilibrium with $Mg(OH)^+$ on the surface of MgO. Magnesium ions get dissolved into the solution as OH^- anions get desorbed from the surface. When supersaturation has been reached, magnesium hydroxide starts to precipitate on the surface of MgO [19–21]. Consequently, there is still 30–45 % of unreacted MgO present in the binder after 28 days [22,23] which could react later to form brucite leading to structural instability due to potential crystallization pressure caused by late reaction of MgO. Therefore, solutions to maximize the carbon capturing capacity of the binder are of immediate interest since they will generate a twofold impact: effectively utilize carbon and enhance the durability of the binder.

Organic ligands are known to be effective chelating agents that can steer the reaction pathways and kinetics of MgO-based binders. Magnesium acetate (Mg-acetate) has shown to have a positive effect in increasing the hydration degree of MgO, by facilitating the precipitation of brucite in the bulk solution than on the surface [19,24–26]. Filippou et al. [24] were one of the first to study the rate of hydration of MgO (calcined from $MgCO_3$ at 900 °C) in the presence of magnesium acetate. They suggested that magnesium acetate dissociates to form magnesium ions and acetate in solution (Eq. (1)). The acetate ions then promote the dissolution of MgO through complexation (Eq. (2)) followed by the dissociation of the Mg-acetate complex and precipitation of magnesium hydroxide due to supersaturation (Eqs. (3) and (4)).

$$(CH_3COO)_2Mg_{(aq)} \leftrightarrow 2CH_3COO^-_{(aq)} + Mg^{2+}_{(aq)} \quad (1)$$

$$MgO_{(s)} + 2CH_3COO^-_{(aq)} + H_2O \rightarrow CH_3COOMg^+_{(aq)} + 2OH^- \quad (2)$$

$$CH_3COOMg^+_{(aq)} \rightarrow CH_3COO^-_{(aq)} + Mg^{2+}_{(aq)} \quad (3)$$

$$Mg^{2+}_{(aq)} + 2OH^-_{(aq)} \rightarrow Mg(OH)_{2\ (s)} \quad (4)$$

The maximum amount of magnesium hydroxide formed in the presence of 0.1 M magnesium acetate at 80 °C and liquid to solid ratio of 10 was 84 % after 3 h of hydration for a medium reactive MgO, while 66 % $Mg(OH)_2$ was formed in water after about 10 h [19]. The hydrating agents are also known to alter the morphology of $Mg(OH)_2$ to form hexagonal plates with large diameters but with reduced thickness [24,26], which in return, may change the mechanical performance of the materials. Several works from Dung and Unluer [22,27,28] have shown increased carbonation potential and mechanical performance for reactive magnesium cement when Mg-acetate was used as the hydration agent. The increase in the formation of carbonate phases in the presence of Mg-acetate was attributed to the increased formation of magnesium hydroxide, which in turn carbonates to form HMCs. However, there is no clear evidence in the open literature for the role of magnesium acetate in the hydration of a reactive MgO-based binder. The phenomenon remains unclear whether the ligand can alter the reaction products in the binder in addition to steering the hydration kinetics. Furthermore, the role of acetate during carbonation is investigated to assess if the reaction rate and degree, as well as the HMCs formed, are altered or if its role is limited to increasing the amount of hydration product and hence would be the focus of this study.

To this end, the hydration and carbonation of MgO in water and magnesium acetate solution (0.05 M to 0.5 M) were studied. The hydration of MgO in different hydrating media and their reaction products including magnesium hydroxide and hydrated magnesium carbonates (HMCs) resulting from the carbon curing were investigated. The research output will provide key insights into the reaction mechanisms of the MgO-based binder in the presence of acetate ligand. This leads to a deeper understanding of approaches to optimize carbon capture and utilization processes as well as the practical applications in producing low-carbon MgO-based binders.

2. Materials and methods

2.1. Materials

Magnesium oxide (MgO) was prepared in the laboratory by calcining magnesium hydroxide ($Mg(OH)_2$) from VWR chemicals (assay 95–100.5 %) in a static furnace at 900 °C for 6 h. The calcining temperature and duration were chosen to get a reactive magnesium oxide [29]. Magnesium acetate tetrahydrate ($Mg(CH_3COO)_2.4H_2O$) was obtained from Sigma-Aldrich (assay ≥99 %) and used without further treatment to prepare solutions with targeted concentrations. The chemical composition of MgO from X-ray fluorescence (XRF) is given in Table 1. The particle size distribution of calcined MgO as obtained from laser diffraction spectroscopy is shown in Fig. 1a. The median particle diameter (d_{50}) was observed to be 3.5 μm. The surface area of the MgO was measured to be 11.4 m^2/g using BET. The X-ray diffraction pattern of the calcined MgO is shown in Fig. 1b. The reactivity of calcined MgO was measured using the citric acid test. The time required for neutralizing 2 g of MgO in 100 ml of 0.40 N (0.133 M) citric acid solution by phenolphthalein was 202 s, which corresponds to medium reactive MgO [25].

2.2. Methods

2.2.1. Sample preparation

Paste samples were cast with a water/solid (w/s) ratio of 1 to achieve the necessary workability. MgO was mixed with 0.05 M, 0.1 M, and 0.5 M magnesium acetate solution. A mix with demineralized water was taken as the control mix. Mg-acetate solutions with different concentrations were prepared and equilibrated at least 24 h prior to their use. The Mg molar concentration was kept constant for all mixes and the mix design is shown in Table 2.

A schematic representation of sample preparation is shown in Fig. 2. The paste was mixed using a shear mixer for 5 min at 800 rpm, cast in 40 ml vials (2.5 cm diameter) on a vibrating table, and cured for 24 h in the closed vials. Once the samples were demoulded after 24 h, they were cut into thin discs of 3–5 mm thickness and diameter of 2.5 cm. For hydration experiments, the samples were placed in a humidity chamber at 25 ± 0.5 °C temperature and 98 % ± 2 % RH. Carbonation was done at 23 ± 2 °C in a desiccator with a saturated solution of NaCl to maintain the RH of about 70 % ± 5 %. Lower relative humidity was used compared to hydration experiments since high RH would hinder the

Table 1
Chemical composition from X-ray fluorescence spectroscopy (XRF).

Oxide composition (%)	MgO	SiO_2	SO_3	CaO	LOI (Loss on ignition at 950 °C)
MgO (obtained after $Mg(OH)_2$ calcination)	99.73	0.02	0.08	0.1	0.6

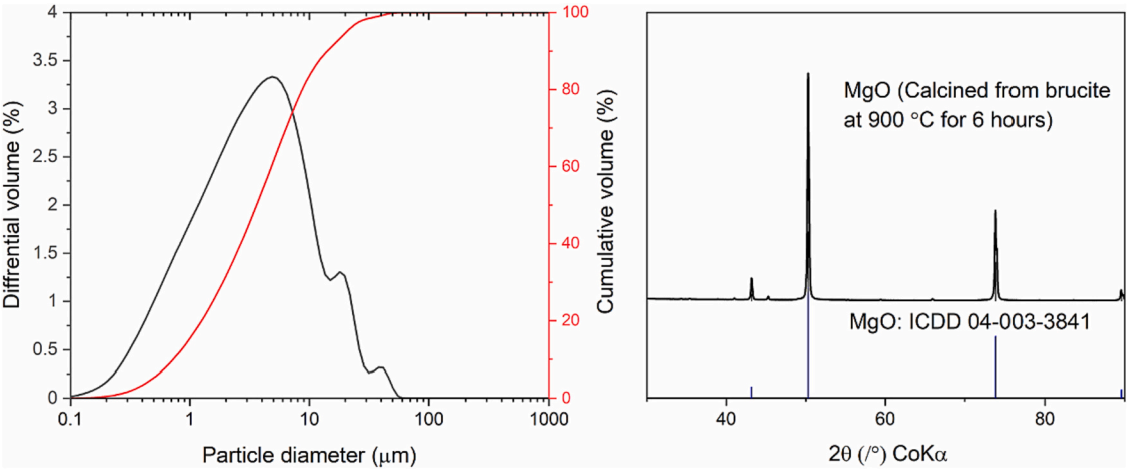

Fig. 1. (a) Particle size distribution and (b) X-ray diffraction pattern of calcined MgO.

Table 2
Mix recipe used in the study. The MgO content was adjusted to have a constant molar concentration of Mg in all mixes.

Sample	MgO (g)	H_2O (g)	Mg-Acetate solution[a] (g)	Water-to-solid -ratio
Ref-0 M	20	20	–	1
0.05 M	19.96	–	20	0.99
0.1 M	19.92	–	20	0.98
0.5 M	19.60	–	20	0.88

[a] Corresponds to respective sample concentrations.

carbonation process. The CO_2 gas (purity ≥99.8 %) released at a pressure of 1 bar ($T = 23 \pm 2$ °C) was flushed into the desiccator once every 24 h for 15 mins and the rate of the gas flow was controlled by a flowmeter at 65 cc/min. The samples were collected after 1, 7 and 28 days of curing. Further reaction was stopped using the solvent exchange method [30,31]. The discs were broken into small pieces and immersed in isopropanol for 24 h, the solvent was changed after the 1st hour. The samples were then placed in an oven at 40 °C for 2.5 h to completely evaporate the solvent. The full slice of the sample was then crushed to fine powder gently with mortar and pestle to get a representative mix from both the surface and bulk of the carbonated sample for all analyses including XRD, TGA, SEM and total carbon measurements. The samples were stored in air-tight containers, before further analysis.

2.2.2. Isothermal calorimetry

MgO (2 g) was mixed by hand using a spatula with the hydrating solution at w/s = 1 before placing it in the calorimeter. An isothermal calorimeter TAM Air (TA instruments) was used to measure the hydration heat flow at 23 °C. Prior to the measurement, the temperature was set and stabilized for 24 h. The heat flow was recorded after 15 min from the instance of placing the sample in the calorimeter. An equivalent quantity of the respective hydrating solution was used as the reference solution. The heat flow was measured for 5 days. After the experiment ended, the ampoule was removed from the instrument and the final baseline was made by stabilizing the temperature for 30 min. The integration of the heat flow curves was determined after 15 min from the instance of placing the sample in the calorimeter.

2.2.3. X-ray diffraction

X-ray powder diffraction (XRD) was performed using a Rigaku SmartLab equipped with a Co Kα source (Kα1 = 1.78892 Å; Kα2 = 1.79278 Å; Kα1/Kα2 = 0.5) operated at 40 kV and 135 mA. The measurements were conducted at a scan rate of 3°/min in the range 5° to 90° 2θ with a step size of 0.02°/step. About 10 wt% zincite was added as an internal standard to enable quantification of the amorphous content. Phase identification and Rietveld quantitative phase analysis were carried out using the High Score software integrated with PDF 4+ 2022 database. The crystal structure models for the identified phases were taken from the literature [32–35]. The global variables including the background and specimen displacement were refined. The available background was used to refine the background. The scale factors, the lattice constants and peak profile parameters were refined. The peak shape and the width were modeled using the pseudo-Voigt function and the Caglioti function, respectively. Preferred orientation correction was

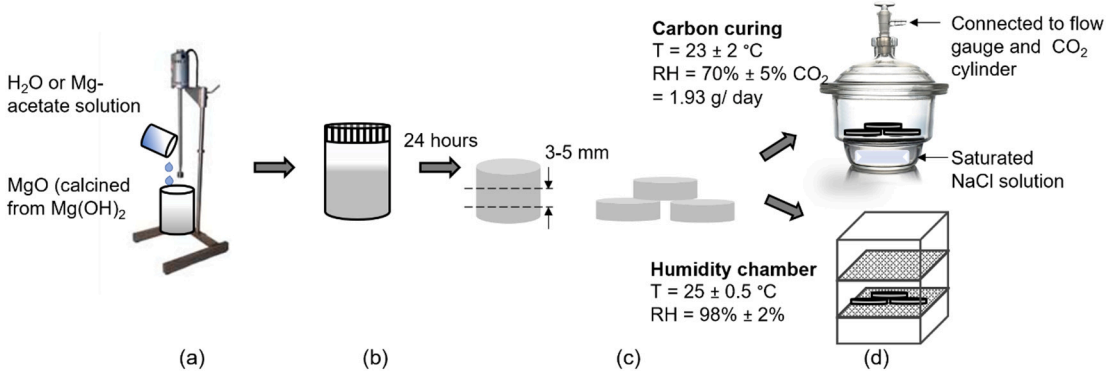

Fig. 2. Schematic representation of sample preparation and curing conditions. (a) Calcined MgO was mixed with the hydrating solution (w/s = 1) (b) the paste was cast in a 40 ml vial and (c) after 24 h of curing, the samples were demolded and cut into thin slices. (d) The cut slices were cured in two environments; hydration was done using a humidity chamber and carbon curing in a desiccator.

applied to nesquehonite using the March-Dollase function. The quantified results were then recalculated according to [36] to 100 g anhydrous binder.

The Scherrer equation (Eq. (5)) was used to calculate the crystallite size (D). Where λ is the wavelength of the X-ray used (1.7889 Å), K is the Scherrer constant and depends on the crystallite size and shape (K = 0.94). θ is the diffraction angle and β corresponds to the full width at half maximum (FWHM) of the broadened diffraction peak. It was assumed that instrument broadening was negligible.

$$D = \frac{K\lambda}{\beta cos\theta} \quad (5)$$

2.2.4. Thermal analysis

A DSC-TG (SDT 650, TA instruments) was used to measure the decomposition of hydrated samples. The temperature was increased from 30 °C to 980 °C with a ramp of 10 K/min. About 20 mg of sample were loaded in an alumina crucible, and N_2 atmosphere with a flow rate of 100 ml/min was used. Selected samples were analyzed using thermogravimetric measurements coupled with infrared spectroscopy (Netzsch STA 449 F3 Jupiter TGA coupled with a Bruker Fourier-transform infrared spectrometer). CO_2 and H_2O in the exhaust gas were measured as a function of absorbance in the range of 2200–2450 cm^{-1} and 1300–2000 cm^{-1}, respectively.

2.2.5. Scanning electron microscopy

The morphologies of the pastes were studied using JEOL field emission scanning electron microscopy (FESEM). An accelerating voltage of 5 kV and a working distance of about 10–15 mm were used. The images were taken using secondary electron mode. Platinum coating at 40 mA for 40 s was done to reduce charging.

2.2.6. Total carbon measurement

The total carbon content was measured using CS-200 carbon and sulfur analyzer (LECO corporation). About 200–300 mg of powdered sample was heated and combusted in O_2 atmosphere. The carbon and sulfur emitted from the sample were oxidized to CO_2 and SO_2. The gases were detected with a coupled IR module. Calibration was done with reference samples with known carbon contents. The measurements were done in triplicates for repeatability.

3. Results

3.1. Hydration of magnesium oxide

The heat of hydration of calcined MgO in water and magnesium acetate solution is shown in Fig. 3. The cumulative heat flow is normalized per gram of MgO in the mix. The addition of Mg-acetate significantly accelerated the hydration of MgO, which is in line with the previous works [24,25]. With the increase in the concentration of Mg-acetate solution, the rate of hydration increases. The cumulative heat after 72 h is higher for the samples with acetate than for the reference. It can be noted further that the cumulative heat release for the sample with 0.5 M Mg-acetate solution is lower compared to the intermediate concentrations of Mg-acetate solution and is discussed further in Section 4.1. The first 30 min of MgO hydration in 0.5 M Mg-acetate contributes to about 15 J/g of heat of hydration and can therefore be neglected (see Section A1 in the appendix for more details).

The morphology of the hydration products formed with and without Mg-acetate after 24 h of curing is shown in Fig. 4. Images of samples after 28 days of hydration are provided in Fig. A2 in the Appendix. The increased rate of formation of brucite in the Mg-acetate solution seems to have resulted in a different morphology than in the reference. Hexagonal platelets of brucite are formed in the mix with water, as observed in Fig. 4a, whereas in the presence of Mg-acetate thin sheet-like layers of larger diameter are formed. Different morphologies of brucite have been reported in the past [24,26,37,38], and are suggested to be influenced by the reactivity of MgO, addition of seeding agents and the hydrating agent used.

Fig. 5 shows the thermal decomposition of MgO paste hydrated with different concentrations of Mg-acetate cured for 1 and 28 days determined by TG. The thermal decomposition of brucite occurs around 400 °C [39,40]. When MgO is hydrated in water (ref-0 M), brucite decomposition occurs at 375 °C after 1 day and with increased curing time at 400 °C. As expected, the amount of brucite increases with time. With the addition of Mg-acetate, the decomposition of brucite occurs at lower temperatures, even though the amount of brucite formed is high compared to the reference. With increasing concentration of Mg-acetate from 0.05 M to 0.5 M the decomposition of brucite shifts towards lower temperature. It could be noted that the dehydroxylation of brucite formed in the presence of 0.05 M Mg-acetate occurs over a broad range with DTG peaks at 375 °C and 330 °C. In addition, a dehydration peak appears around 405 °C for the sample with 0.5 M Mg-acetate after 24 h of hydration, which does not significantly vary even after 28 days. This

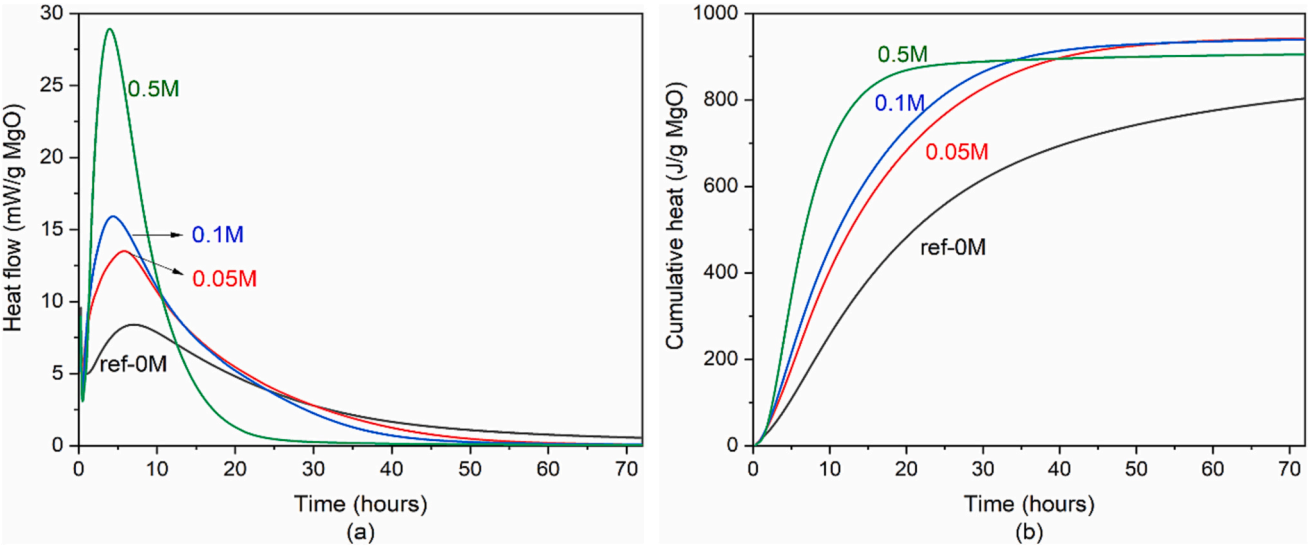

Fig. 3. a) Heat flow and b) cumulative heat of MgO hydrated with water and magnesium acetate solution.

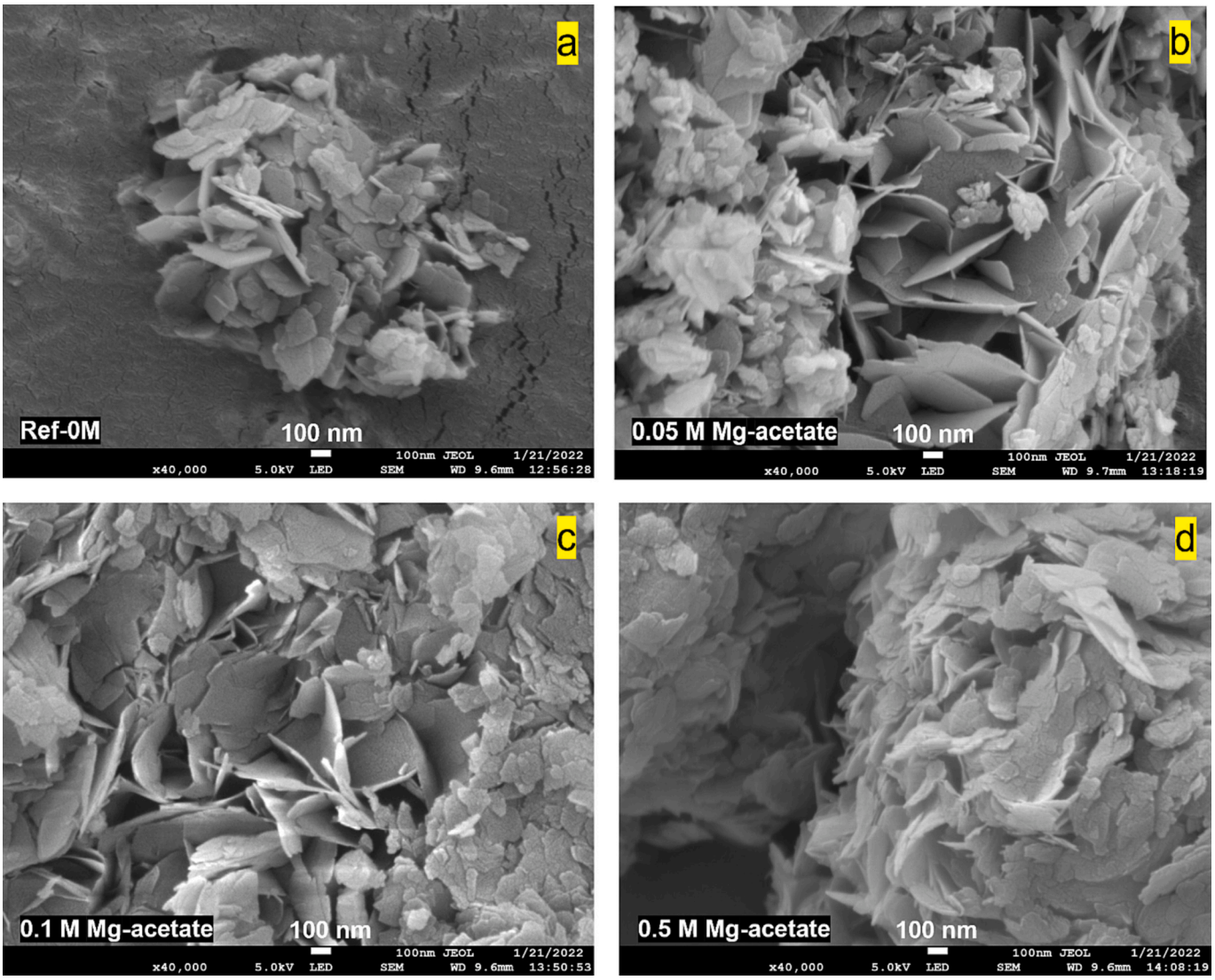

Fig. 4. Morphology of brucite formed after 24 h of hydration in (a) water, (b) 0.05 M Mg-acetate, (c) 0.1 M Mg-acetate and (d) 0.5 M Mg-acetate.

peak is not found in calcined MgO and for lower concentrations of Mg-acetate. Measurements from TG-IR showed both dehydration and decarbonation at 405 °C, indicating either the formation of hydrated carbonate phase or the presence of acetate. The thermal decomposition of Mg-acetate has been reported to be around ca. 360 °C [41].

The phase assemblages of the paste samples analyzed using XRD are shown in Fig. 6. The degree of hydration of MgO increases in the presence of magnesium acetate after 24 h of curing. About 50 mass-% of unreacted MgO remain after 1 day of hydration in the reference sample. However, after 28 days, only a trace of MgO remained. The amount of brucite formed in the presence of Mg-acetate after 1 day increases with the concentration of Mg-acetate. Complete hydration of MgO within 24 h of hydration with 0.5 M Mg-acetate indicates the increase in hydration kinetics of MgO in the presence of Mg-acetate, in line with the observations from isothermal calorimetry (Fig. 3). With 0.5 M Mg-acetate a series of reflections at 8.9, 13.8, 18.8 and 22.8° 2θ CoKα with d-spacings of 11.5, 7.3, 5.5 and 4.5 Å, respectively, are observed after 1 day of curing. The 001 reflection is split into two reflections indicating a distorted crystal structure in the respective crystallographic direction. However, with increased curing time, the reflections tend to shift closer to 20.7 2θ (4.96 Å) and 22.1 2θ (4.67 Å) after 28 days of curing and merge at 21. 8 2θ (4.71 Å) after 3 months of curing (Fig. 12d, discussed further in Section 4.1).

Brucite shows broader reflections with increasing concentration of Mg-acetate, which can probably be related to a change in crystallite size. The average crystallite size of brucite calculated from Scherrer's formula at three different (hkl) planes is shown in Fig. 7. It tends to reduce with increasing concentration of Mg-acetate along all three planes. The uncertainty in the calculated crystallite size can arise from the variation in Scherrer constant K that depends on the crystallite shape, size distribution and the function used to fit the peak profile (FWHM) and therefore, is only an approximate estimation [42,43].

3.2. Carbonation of hydrated MgO

This section presents the results of the subsequent carbonation of brucite formed from MgO after 24 h of hydration. The uptake of CO_2 was measured using the CS-analyzer. Fig. 8a shows the contents of CO_2 in the hydrated MgO pastes cured with water and Mg-acetate solutions, respectively. The CO_2 content as shown in Fig. 8a has been corrected by subtraction with the carbon content of the sample prior to carbon curing and is given in section A2 in the Appendix. The CO_2 uptake of MgO in water (ref-0 M) is higher than in the presence of Mg-acetate and reaches a plateau after 7 days of carbonation curing. With higher concentrations of Mg-acetate (0.1 M and 0.5 M), carbonation continues beyond 7 days. Cracks were observed for the mix with the highest concentration of

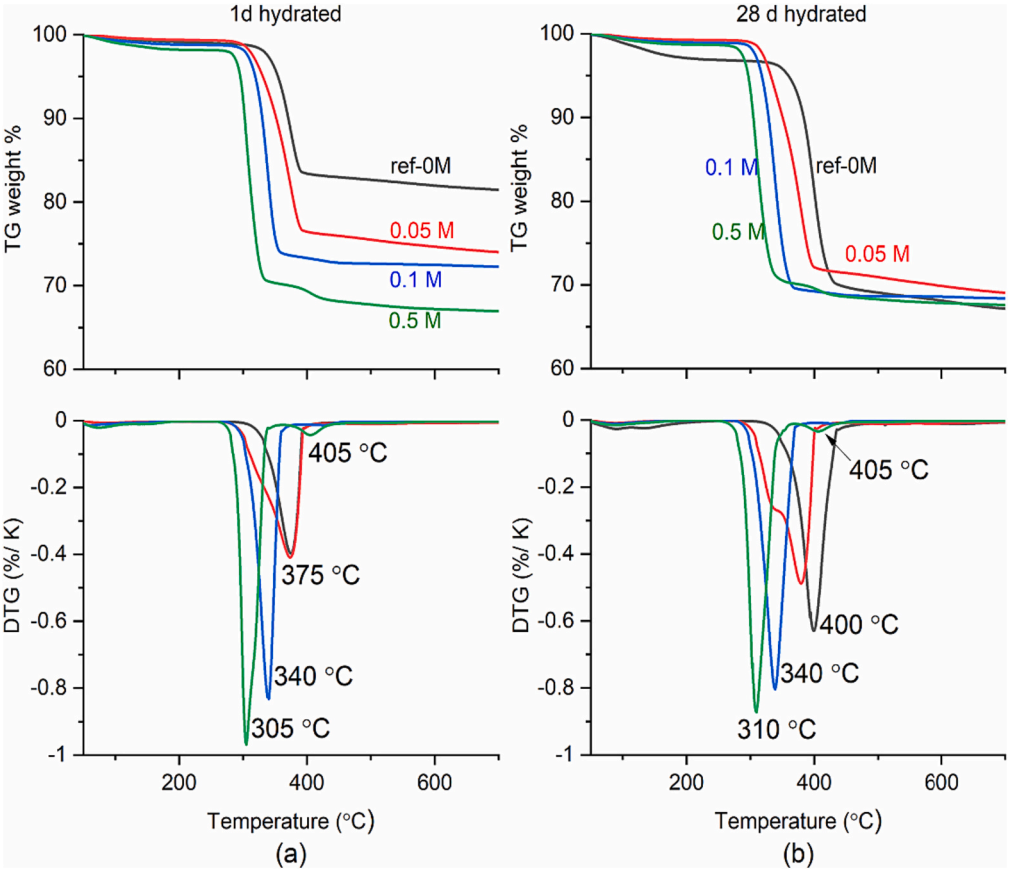

Fig. 5. Thermogravimetric analyses of pastes with different concentrations of Mg-acetate cured for (a) 1 day and (b) 28 days.

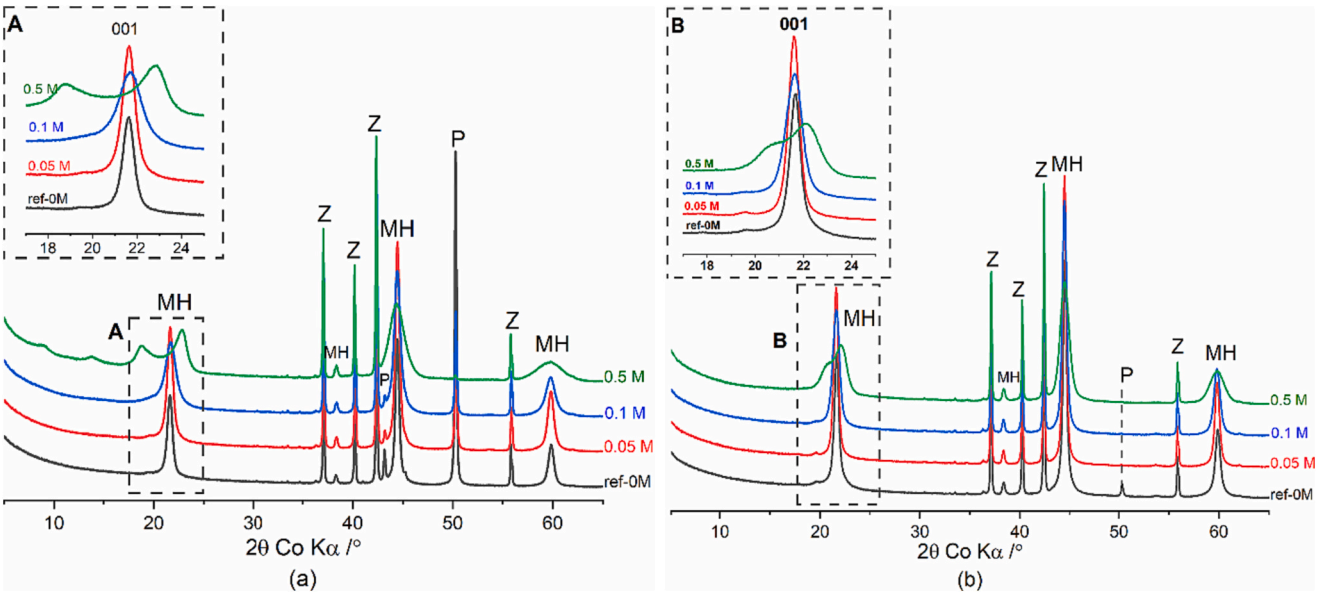

Fig. 6. XRD patterns of MgO hydrated in water and Mg-acetate solution (a) cured for 1 day and (b) hydrated for 28 days (MH-Brucite, *Z*-Zincite (added internal standard), P-Periclase (MgO)). Insert A and B correspond to the angular region of the brucite (001) plane.

organic additive after 24 h of hydration (Fig. 8b), which could explain the increased degree of carbonation compared to the mix with 0.1 M Mg-acetate solution.

The TG-IR analyses of paste samples carbonated for 1 and 28 days in water and 0.5 M Mg-acetate solution, respectively, are presented in Fig. 9. The dehydroxylation of brucite occurs around 300–500 °C and overlaps with the decarbonation range of hydrated magnesium carbonates [40]. Dehydration of nesquehonite ($MgCO_3{\cdot}3H_2O$) occurs in the range of 60 to 250 °C. A strong dehydration peak around 150 °C with shoulders at 105 and 180 °C is observed for the paste without the addition of organic ligand, which corresponds to dehydration of nesquehonite. The mass loss around ca. 420 °C and 520 °C with a hump

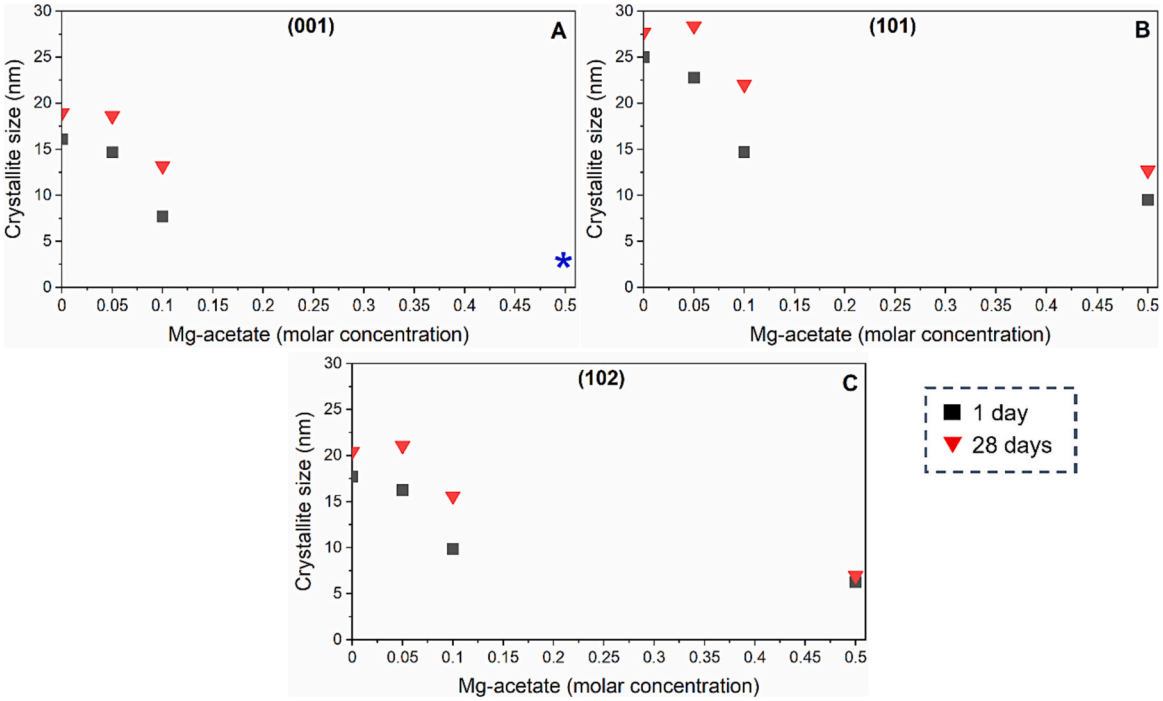

Fig. 7. Crystallite sizes of brucite formed after 1 and 28 days of hydration in different concentrations of Mg-acetate for 3 different crystallographic planes (hkl). The uncertainty in the calculated values is about 13 %, considering K varies from 0.89 to 1. * In A indicates that the crystallite size for 0.5 M Mg-acetate parallel to the crystallographic direction [001] was not calculated due to the splitting of the reflection.

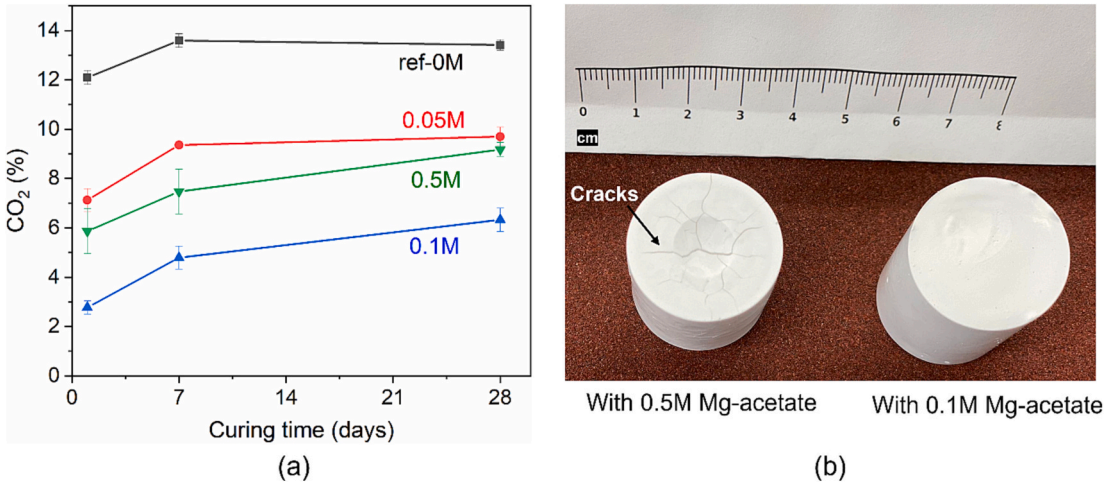

Fig. 8. (a) Amount of CO_2 uptake calculated from the measured total carbon using the CS-analyzer. (b) Development of cracks after 24 h of hydration in the mix with 0.5 M Mg-acetate solution. The cylindrical samples were further cut into thin slices of 3–5 mm before subjecting to carbonation.

around 475 °C is attributed to decarbonation of nesquehonite (similar to [44]).

After one day of carbonation in the presence of acetate, dehydroxylation of brucite occurs at 330 °C. In addition, the mass loss at ca. 100–200 °C is attributed to both dehydration and partially the decarbonation of HMCs, which takes place at relatively low temperatures [40]. Further decarbonation also occurs in a range of 200–450 °C, while dehydroxylation is seen at about 410 °C. There is no clear trace of specific HMCs formed in the samples after 1 day (see Fig. 9b), hence these findings indicate the presence of an amorphous carbonate in the sample after 1 day of carbonation. However, after 28 days, the dehydroxylation of brucite occurs at 360 °C. The mass loss at 120 °C can be attributed to dehydration of giorgiosite-like phase (seen in XRD shown in Fig. 10b). The mass loss at 360 and 415 °C indicates decarbonation of giorgiosite and partially of the amorphous magnesium carbonates and dehydroxylation of the above-mentioned phases occurs at ca. 220 °C and 415 °C. Similar thermal behavior was observed by Nguyen et al. [40] for giorgiosite with predominant dehydration at 127 °C, dehydroxylation at about 300 and 390 °C, and decarbonation also at around 300 °C.

The phase assemblage of samples carbonated for 1 and 28 days obtained from XRD is shown in Fig. 10. A high amount of MgO remains unreacted in the mix with just water compared to the mixes with magnesium acetate solution after 1 day of hydration. Brucite, magnesium oxide and nesquehonite are the phases present in the mix with water. The amount of unreacted magnesia and brucite reduces with the increase in curing time.

For paste samples with 0.5 M Mg-acetate as hydrating agent, no clear reflections of carbonate-bearing phases are observed after 1 day of

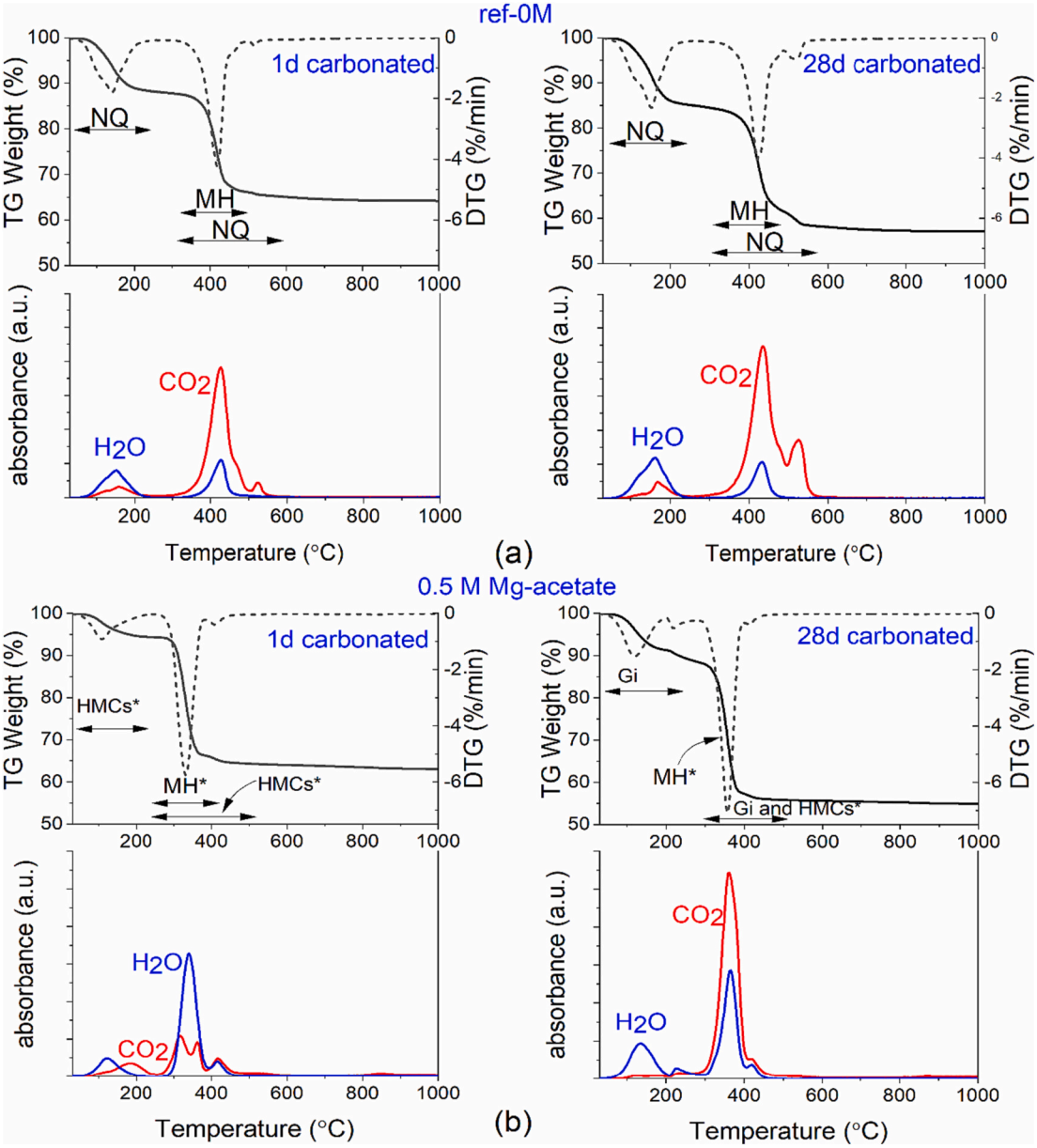

Fig. 9. TG-IR analysis of paste carbonated for 1 day and 28 days in (a) water and (b) 0.5 M Mg-acetate solution. NQ- nesquehonite, MH- brucite, MH*- low crystalline brucite, Gi- giorgiosite-like phase, HMC* indicates possible amorphous HMCs present.

carbonation. After 24 h of carbonation, a series of reflections at 8.9 (11.5 Å), 13.8 (7.3 Å), 18.8 (5.5 Å) and 22.8° (4.5 Å) 2θ CoKα are observed, and the diffraction pattern shows the same reflections prior to carbonation (after 24 h of hydration). However, an unknown reflection at 27.7° 2θ (3.73 Å) is observed after 1 day but is not present after 28 days of CO_2 curing. After 28 days the reflection at 8.9° 2θ CoKα shifts to 8.7° 2θ (11.78 Å), which indicates the presence of giorgiosite-like phase [40]. The intensity of the reflection at 18.8° 2θ CoKα reduces with increased curing time. The samples with intermediate dosages of Mg-acetate do not show clear reflections of carbonate phases even after 28 days of curing.

The morphologies of the paste samples carbonated for 28 days are shown in Fig. 11. The formation of nesquehonite in the system with water is evident from Fig. 11a, which is in accordance with the XRD analysis. With the addition of magnesium acetate, the microstructure changes, and the difference in brucite morphology is evident from Fig. 11c, however, no clear identification of the carbonated phases is possible. In the case of 0.5 M Mg-acetate a dense microstructure (Fig. 11e) can be observed.

4. Discussion

4.1. Effect of acetate on hydration

The crystal structures of brucite and the structure of acetate ion are shown in Fig. 12a and b, respectively. The rate and degree of MgO hydration in water are limited due to the formation of brucite on the surface of MgO [45]. However, as given in Eqs. (1) to (4), Mg-acetate facilitates the precipitation of brucite in the bulk. It is evident from Fig. 3 that with an increase in acetate concentration, the rate of hydration of MgO increases. The degree of hydration after 24 h is observed to be 56 %, 78 % and 86 % in water, 0.05 M, and 0.1 M Mg-acetate solution, respectively, considering the heat of hydration of MgO to $Mg(OH)_2$ to be 930 J/g [46]. The cumulative heat release is low compared to the above-mentioned heat of hydration of MgO with 0.5 M Mg-acetate solution. However, it is evident from XRD analyses (Fig. 6a) that

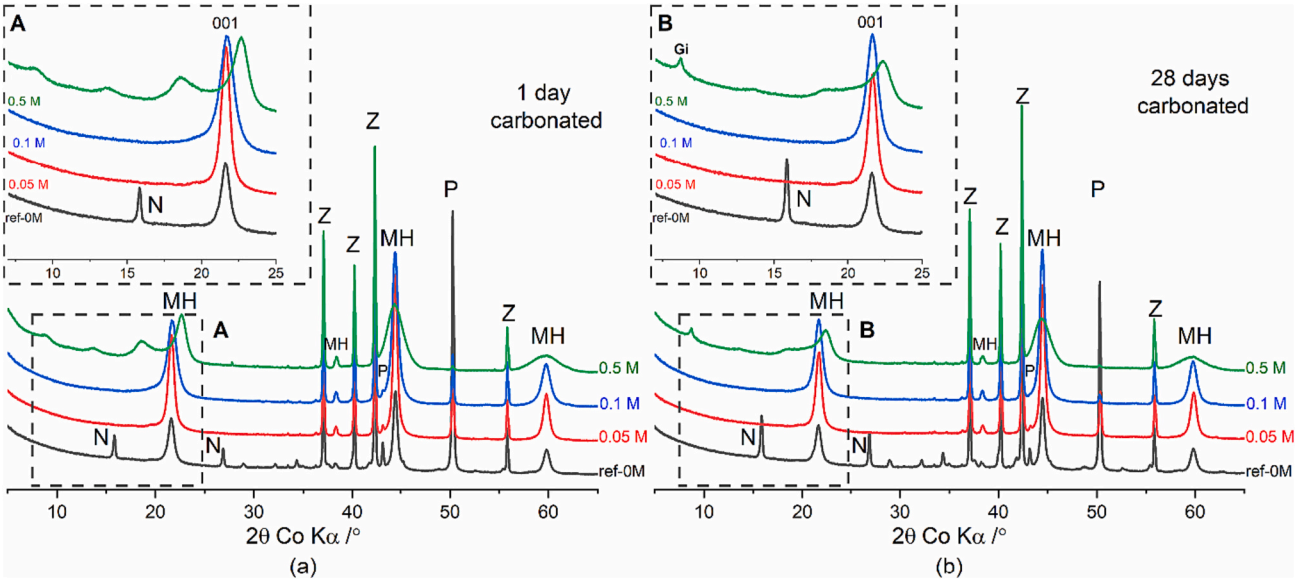

Fig. 10. Phase assemblage of pastes hydrated different hydrating agents and carbonated for (a) 1 day and (b) 28 days (MH-Brucite, *Z*-Zincite (added internal standard), P-Periclase (MgO), N-Nesquehonite and Gi-Giorgiosite) as determined by XRD.

complete hydration of MgO occurs in the presence of 0.5 M Mg-acetate after 24 h of hydration. Thus, the decrease in cumulative heat could be attributed to the difference in enthalpy or hydration energy of MgO in water and Mg-acetate. Several studies have focused on modeling the hydration kinetics of MgO [13,21,24,46,47]. The activation energy of MgO (calcined at 900 °C) hydrated in Mg-acetate was estimated to be 60 kJ/mol by shrinking-core model [24]. Thomas et al. [46] reported the activation energy of technical grade light burned MgO in water to be 77 kJ/mol by fitting the calorimetric data to a boundary nucleation and growth model. This value is in good agreement with the value calculated from the instantaneous method proposed by [48]. Though the activation energies have been calculated using different methods and cannot be directly compared, it can still indicate that Mg-acetate lowers the activation energy suggesting different reaction rates. The change in morphology of brucite as seen from Fig. 4 shows the influence of acetate on the morphology of precipitated brucite. With acetate, the brucite precipitates as thin sheet-like layers of a few nm thickness but larger in diameter (Fig. 4). It has also been previously reported that hydrating agents can alter the morphology of $Mg(OH)_2$. The rapid formation of hydration products in acetic acid or magnesium acetate solution forms thinner platelets compared to the hexagonal crystals of magnesium hydroxide [26]. A schematic representation of magnesium hydroxide precipitated in water and 0.5 M Mg-acetate is shown in Fig. 12c. The thickness of the mineral shown in the figure is calculated from multiple SEM images using ImageJ software, and therefore is a representative value. The brucite precipitated in the presence of Mg-acetate seems to have a rather nanocrystalline structure, and acetate seems to alter the growth of the crystal along the [001] direction.

Though MgO hydrates to form brucite both in water and acetate solution, it is evident from the obtained results that the properties of the brucite, in either case, differ quite significantly. The shift in the thermal decomposition of brucite to lower temperature (Fig. 5) indicates lower particle size and/or lower crystallinity of brucite that is formed in the presence of Mg-acetate. Co-precipitation of organic substances with different minerals is known to affect the crystallinity of the precipitates [49,50]. The carbon content (C %) of samples after hydration was measured using CS-analyzer and was 0.76 ± 0.01 % and 1.86 ± 0.01 %, for water and 0.5 M Mg-acetate solution respectively indicating co-precipitation of acetate with brucite. Formation of a brucite with low crystallinity during hydration of MgO in the presence of hydromagnesite has also been reported [10,37].

The broadening of the XRD reflections of brucite formed with the addition of acetate indicates changes in crystallite size and crystallinity. The crystallite size parallel to different crystallographic directions, namely [001], [101] and [102] presented in Fig. 7 shows the reduction in the size with increasing concentration of acetate. The reduction in crystallite size after 28 days of hydration compared to the brucite precipitated in water (ref-0 M) is approximately 20 % parallel to [101] and [102] for 0.1 M and approximately 60 % for 0.5 M Mg-acetate solution, respectively. However, the reduction in crystallite size is less pronounced along directions parallel to the crystallographic c-axis. Furthermore, the 001 reflection of brucite formed in the presence of 0.5 M acetate concentration after 24 h of hydration (Fig. 6a) is split into two distinct reflections with d-spacings of 5.5 Å and 4.5 Å, which are higher and slightly lower than the d-spacing of brucite (4.77 Å). Similar observations of such a split in d-spacing have been reported for layered double hydroxides (LDH) from brucite-type structure ($M^{2+}(OH)_2$) [51] and intercalation of organic or inorganic anions in Mg-Al LDH [52,53], which were attributed to different staging/segregation phenomena. Further, Bernard et al. [53] have observed splitting of the 003 reflection of hydrotalcite intercalated with sulphate anions into two distinct peaks, one higher and lower than the basal spacing reported for the pure phase. The authors attributed this effect to a swelling of the interlayer by incorporation of water along with SO_4^{2-} anions, and replacement of SO_4^{2-} anions by carbonate impurities (CO_3^{2-} anions) in the interlayer respectively.

The evolution of d-spacing parallel to [001] direction with aging up to 3 months for MgO hydrated in 0.5 M Mg-acetate is shown in Fig. 12d. TG data of the paste hydrated in 0.5 M Mg-acetate for 3 months is given in Fig. A3. The broadening of the XRD reflections decreases with increasing curing time, and the splitting and shift of the 001 reflection decreases with time as well. After 3 months of curing, the 001 reflection at 21.8 2θ corresponding to a d-spacing of 4.71 Å is observed and is comparable with the reference brucite. The changes in d-spacing with the increase in temperature to simulate aging have been reported to be the result of the reorientation of anions in the interlayer to stable states or removal of molecules from the interlayer [52,53]. It could be concluded that hydration of MgO in the presence of Mg-acetate, precipitates brucite with distorted crystal structure. The acetate interacts with the hydration product, alters the pathway of crystallization eventually the crystal growth, leading to thin sheet-like morphology. Similar effects were seen with the presence of poly(acrylic acid) that alters the

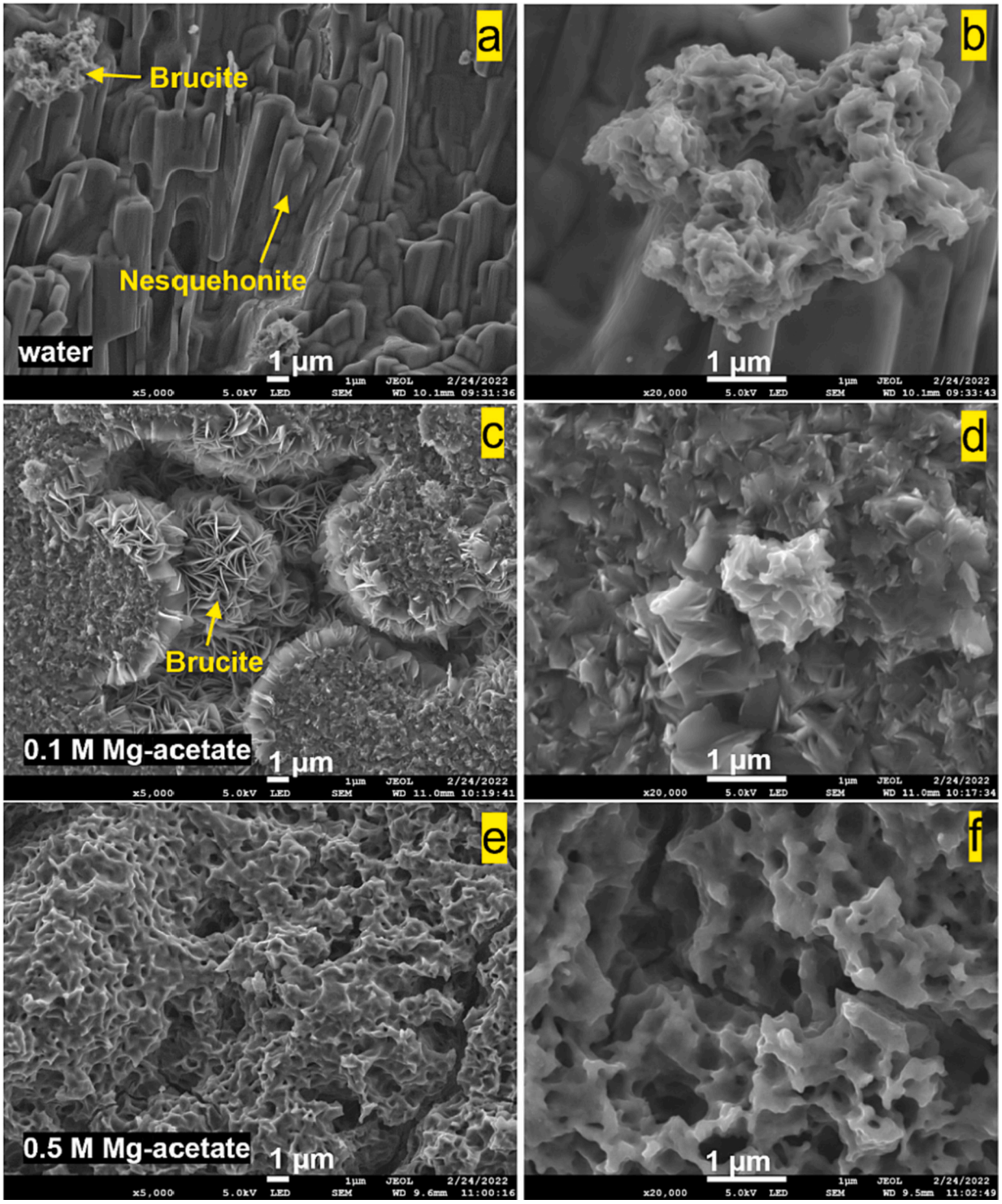

Fig. 11. SEM micrographs of fractured MgO paste carbonated for 28 days in water (a, b), 0.1 M (c, d) and 0.5 M Mg-acetate solution (e, f).

growth of brucite in an aqueous solution and forms nanoplatelet morphology than the hexagonal morphology of brucite [54].

Further, the observations from the diffraction pattern (after 24 h of hydration) together with lower heat of total hydration in the case of 0.5 M Mg-acetate suggests that the brucite formed is not the most stable structure and impurities such as acetate ions may have been trapped between the MgO_6 octahedral layers and could explain the increase in d-spacing. The changes in reflection of the 001 plane with increased curing time indicate the recrystallization of brucite to a more stable crystal structure over time along with the removal of ions from the interlayer. The acetate ions removed from the precipitates could be present in the pore solution and needs more study. However, the exact position of acetate in the crystal structure together with the underlying mechanisms will be the subject of further studies.

4.2. *Effect of acetate on carbonation*

The samples were demolded (after 24 h of hydration) and carbon cured for 1, 7 and 28 days. On carbonation, brucite reacts to form different hydrated magnesium carbonates (HMCs) based on the reaction

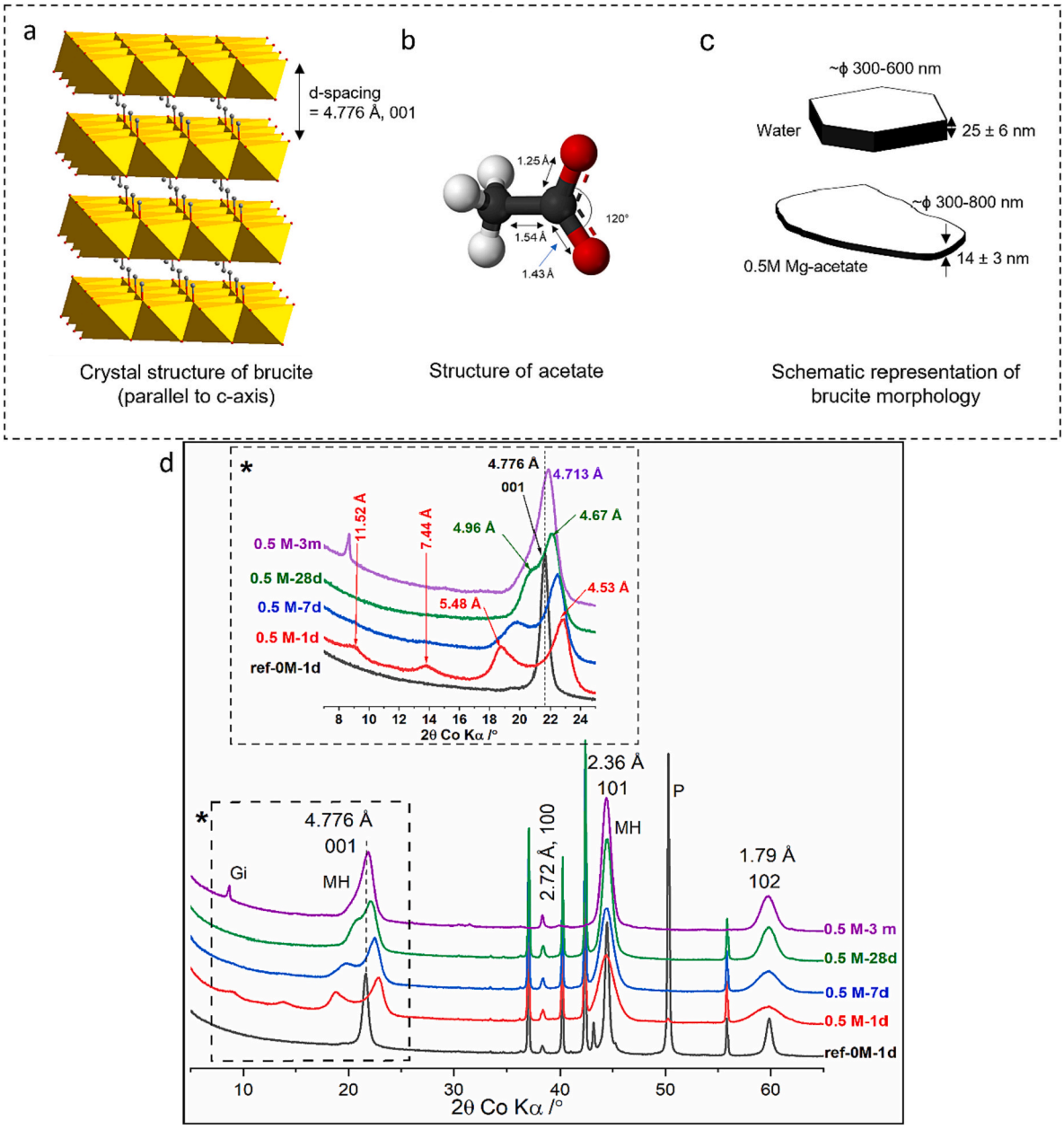

Fig. 12. (a) Layered structure of brucite parallel to crystallographic c-axis and (b) structure of acetate ion (not to scale). (c) Schematic representation of the morphology of brucite formed in water and 0.5 M Mg-acetate solution and (d) diffraction pattern of MgO hydrated in 0.5 M Mg-acetate for different curing times and MgO hydrated in water for 1 day as reference, * is the insert to (d) from 7 to 25 2θ (MH-Brucite, P-Periclase and Gi-Giorgiosite).

conditions. The stability of these materials is still a concern as the HMCs formed are metastable. Brucite and magnesite ($MgCO_3$) are the thermodynamically stable phases at low and high CO_2 concentrations, respectively. However, the formation of magnesite is kinetically hindered at ambient conditions, and it requires elevated temperature and pressure and instead forms a range of HMCs [55]. This is attributed to the high hydrating nature of Mg atoms with 6 coordinated water molecules surrounding Mg^{2+} [56]. The variety of HMCs that could form in MgO-CO_2-H_2O system are barringtonite ($MgCO_3{\cdot}2H_2O$), nesquehonite ($MgCO_3{\cdot}3H_2O$), lansfordite ($MgCO_3{\cdot}5H_2O$), hydromagnesite ($Mg_5(CO_3)_4(OH)_2{\cdot}4H_2O$), dypingite ($Mg_5(CO_3)_4(OH)_2{\cdot}5H_2O$), artinite ($Mg_2(CO_3)(OH)_2{\cdot}3H_2O$), pokrovskite ($Mg_2(CO_3)(OH)_2$), giorgiosite ($Mg_5(CO_3)_4(OH)_2{\cdot}5–6H_2O$). Which phase predominantly forms depends mainly on temperature and CO_2 pressure, however, various other factors such as pH or water activity have also been reported to be relevant [55].

In the system with MgO and water, nesquehonite forms as the carbonation product along with unreacted magnesium hydroxide and unreacted MgO, as observed from XRD (Fig. 10) and TG-IR (Fig. 9a). In addition, an amorphous content of 34 mass- % and 56 mass- % after 1 and 28 days were quantified by Rietveld refinement. About 40 mass- % of unreacted MgO and 48 mass- % of brucite remain after 28 days of curing. However, almost complete hydration of MgO after 28 days is observed when the samples were cured in the humidity chamber (Fig. 6b). Formation of HMCs around unreacted MgO and brucite is suggested to lead to surface passivation and limits further hydration and carbonation [18,23,57]. The amount of nesquehonite increased from 17 mass- % at 1 days to 30 mass- % after 28 days of CO_2 curing which relates to 5.2 mass-% and 9.5 mass-% of embodied CO_2. However, the higher amount of embodied CO_2 calculated from total carbon content as determined by the CS-analyzer (Fig. 8a) suggests the formation of (intermediate) amorphous carbonate-containing products [58,59]. In the presence of 0.5 M Mg-acetate giorgiosite-like phase along with acetate-

modified brucite are observed after 28 days of curing (Fig. 10b). The formation of giorgiosite, which has a chemical composition to the one of dypingite but with 5–6 water molecules, has been reported previously. Nguyen et al. [40] have observed that in the presence of acetate, nesquehonite transforms in the long term to giorgiosite instead of dypingite. More information about this phase is still needed. No clear indications of other carbonate phases are observed by XRD of the pastes with intermediate concentrations of Mg-acetate. However, results from TG-IR show the presence of carbon-containing phase(s) in those samples. TG-IR of the paste sample hydrated in 0.1 M Mg-acetate solution and CO_2 cured for 28 days is given in Fig. A4. The thermal decomposition around ca. 370 °C corresponds to decarbonation. This indicates the formation of X-ray amorphous (hydrated) magnesium carbonates (AMC) [58]. Thus, it can be concluded that acetate, in addition to modifying the brucite structure, influences the carbonation pathway.

Measurements of the carbon contents by the CS-analyzer (Fig. 8a) show a decrease of the CO_2 content in the presence of Mg-acetate. This could be attributed to one or both of the following reasons; i) the increase in kinetics of hydration of MgO in the presence of Mg-acetate leads to a denser microstructure of magnesium hydroxide. This process is also accompanied by an increase in volume and hence reduces the porosity, leading to decreased diffusion of CO_2. The increase of carbonation degree of the sample prepared with 0.5 M acetate could be due to the formation of surface cracks after 24 h of hydration (Fig. 8b); ii) the rates of carbonation of brucite formed in samples with Mg-acetate and water are different. The presence of magnesium acetate accelerates the formation of magnesium carbonate hydrates, which may precipitate on the brucite surface, inhibiting further reaction. The role of organic and inorganic ligands on the kinetics of brucite dissolution has been studied by Pokrovsky et al. [60]. They found that the effect of acetate on the dissolution of brucite depends primarily on the molar concentration and pH, with neutral or weekly alkaline pH promoting and alkaline pH (>10.5) inhibiting the dissolution. A high concentration of magnesium acetate (1 M) led in their study to a higher amount of acetate sorbed on the brucite surface, leading to an increase in dissolution and thereby increasing the kinetics of brucite carbonation. The complete reaction of brucite in an aqueous environment after 28 days in the presence of acetate was observed by [40] in contrast to 50 % reactivity in neat water. The authors attributed this effect to the lower pH of the liquid phase (9.2 in the presence of acetate, compared to 11 with neat water). An increased degree of carbonation of reactive magnesia cement-based concrete samples (50 mm × 50 mm × 50 mm) with Mg-acetate used as hydration agent was also reported [28], however, it is important to note that the samples used have a higher porosity and pore connectivity than the paste samples studied in this work. The degree and rate of carbonation in paste samples with acetate are limited by CO_2 diffusion into the matrix. From the present study, it can be concluded that the ligand modifies the brucite properties and influences the mineral carbonation pathway. Amorphous magnesium carbonates formed in the intermediate molar concentration of Mg-acetate imply that the nanocrystalline brucite might play a key role in HMCs formed on CO_2 curing.

5. Conclusions

In this study, the hydration and carbonation kinetics and reaction products of MgO in water and Mg-acetate solution were elucidated. The observation provides key insights into the reaction mechanism, kinetics, and degree of MgO hydration in the presence of acetate. It was observed that acetate, in addition to enhancing the hydration kinetics, also modifies the morphology of the precipitated magnesium hydroxide. It could be concluded that the acetate ligand co-precipitates with brucite and alters its crystal structure. Addition of acetate results in nanocrystalline brucite, hindering the crystal growth along the [001] direction. However, with increased concentration (0.5 M) the 001 reflection is split into two reflections, which tend to merge with time. From the observations we propose that the acetate could be present in the interlayers of brucite and with longer curing time, brucite recrystallizes to its stable structure. The formation of hydrated magnesium carbonates on subsequent carbonation of hydrated pastes reveals that acetate along with the modified brucite play a significant role in the carbon mineralization pathway. Nesquehonite is formed in the paste sample hydrated in water and is still stable after 28 days. The presence of acetate leads to the formation of amorphous (hydrated) magnesium carbonates and giorgiosite instead of nesquehonite. The total carbon uptake with the addition of Mg-acetate has decreased compared to the reference system, however, this could be due to other factors like porosity or the formation of a passivation layer and further studies are necessary to optimize the system. Higher concentrations of acetate lead to the formation of cracks in the paste samples and are not recommended for practical applications. Overall, the presence of acetate increases the hydration kinetics and modifies the products of MgO hydration, further influencing the carbon mineralization pathways.

CRediT authorship contribution statement

Nirrupama Kamala Ilango: Conceptualization, Data curation, Formal analysis, Investigation, Methodology, Validation, Visualization, Writing – original draft, Writing – review & editing. **Hoang Nguyen:** Conceptualization, Formal analysis, Methodology, Validation, Visualization, Supervision, Writing – review & editing. **Alexander German:** Methodology, Writing – review & editing. **Frank Winnefeld:** Conceptualization, Methodology, Validation, Supervision, Writing – review & editing. **Paivo Kinnunen:** Conceptualization, Validation, Resources, Supervision, Writing – review & editing, Funding acquisition.

Declaration of competing interest

The authors declare that they have no known competing financial interests or personal relationships that could have appeared to influence the work reported in this paper.

Data availability

Data will be made available on request.

Acknowledgment

The authors would like to acknowledge the financial support from the University of Oulu & The Academy of Finland Profi5 326291, as well as the Academy of Finland project 329477. The authors also appreciate the support from Durgaprasad Ramteke for helping with TG-DSC measurements, Jarno Karvonen and all lab technicians of Fiber and Particle Engineering Unit. A part of the material characterization was carried out with the support of the Centre for Material Analysis, University of Oulu, Finland.

Appendix A.1. Calorimeter

In-situ measurements of heat of hydration of MgO in 0.5 M Mg-acetate solution was done to determine the heat release during the initial few minutes of reaction. The paste was mixed inside the calorimeter for 15 min. A higher water/solid ratio of 1.5 was used to facilitate proper mixing. The heat release during the first 30 min of MgO hydration in 0.5 M Mg-acetate contributed to about 15 J/g to the heat of hydration as measured from in-

situ mixing and is therefore negligible.

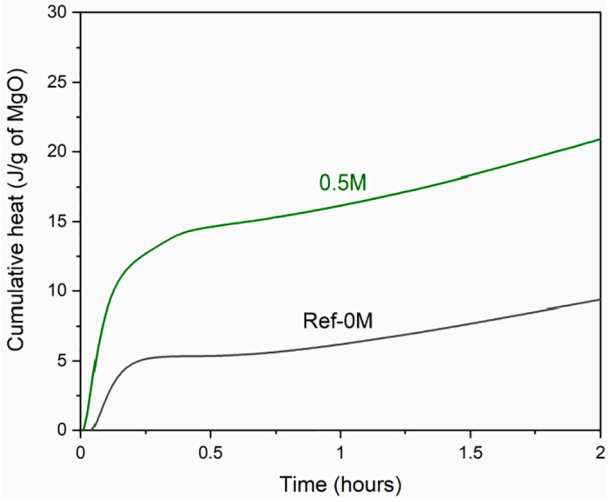

Fig. A1. Cumulative heat of hydration of MgO in water (Ref-0 M) and in 0.5 M Mg-acetate solution for the first 2 h as measured using in-situ mixing method.

Appendix A.2. Carbon content measurement

The carbon content (C %) of samples after hydration (24 h) was measured and was 0.76 ± 0.01 %, 0.68 ± 0.02 %, 0.88 ± 0.01 %, 1.86 ± 0.01 %, for ref., 0.05 M, 0.1 M and 0.5 M Mg-acetate solutions, respectively. The source of carbon in the hydrated samples is from acetate, and due to unavoidable carbonation during sample preparation and curing.

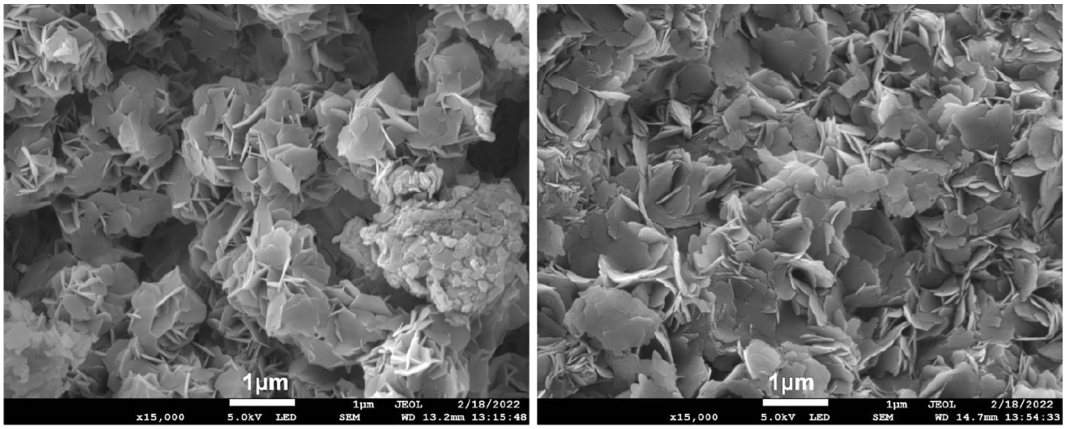

Fig. A2. Morphology of brucite formed in (a) water and (b) 0.5 M Mg-acetate solution (w/b = 1) after 28 days of hydration as determined by SEM.

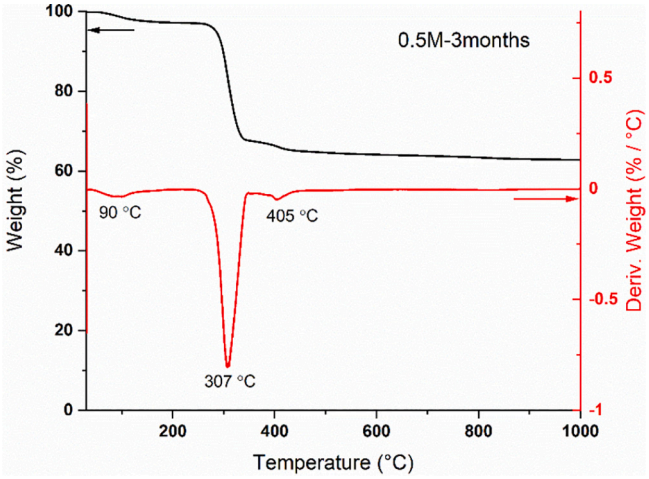

Fig. A3. Thermal decomposition of paste sample hydrated with 0.5 M Mg-acetate solution cured for 3 months.

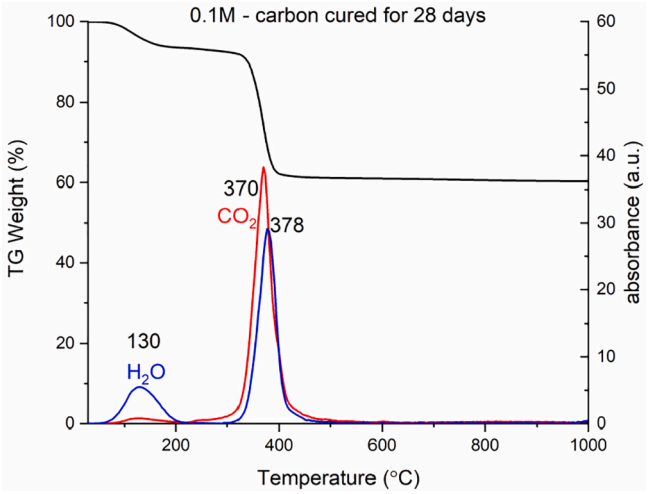

Fig. A4. TG-IR shows the presence of carbonates in the mix with an intermediate concentration of Mg-acetate indicating the presence of amorphous magnesium carbonate.

References

[1] C.R. Gagg, Cement and concrete as an engineering material: an historic appraisal and case study analysis, Eng. Fail. Anal. 40 (2014) 114–140, https://doi.org/10.1016/j.engfailanal.2014.02.004.

[2] C. Lim, E. Jung, S. Lee, C. Jang, C. Oh, K.N. Shin, Global trend of cement production and utilization of circular resources, J. Energy Eng. 29 (2020) 57–63, https://doi.org/10.5855/ENERGY.2020.29.3.057.

[3] K.L. Scrivener, V.M. John, E.M. Gartner, Eco-efficient cements: potential economically viable solutions for a low-CO_2 cement-based materials industry, Cem. Concr. Res. 114 (2018) 2–26, https://doi.org/10.1016/j.cemconres.2018.03.015.

[4] R.M. Andrew, Global CO_2 emissions from cement production, Earth Syst. Sci. Data. 10 (2018) 195–217, https://doi.org/10.5194/essd-10-195-2018.

[5] B. Lothenbach, K. Scrivener, R.D. Hooton, Supplementary cementitious materials, Cem. Concr. Res. 41 (2011) 1244–1256, https://doi.org/10.1016/j.cemconres.2010.12.001.

[6] R. Snellings, Assessing, understanding and unlocking supplementary cementitious materials, RILEM Tech. Lett. 1 (2016) 50–55, https://doi.org/10.21809/rilemtechlett.2016.12.

[7] E. Gartner, T. Sui, Alternative cement clinkers, Cem. Concr. Res. 114 (2018) 27–39, https://doi.org/10.1016/j.cemconres.2017.02.002.

[8] C. Shi, B. Qu, J.L. Provis, Recent progress in low-carbon binders, Cem. Concr. Res. 122 (2019) 227–250, https://doi.org/10.1016/j.cemconres.2019.05.009.

[9] S.A. Walling, J.L. Provis, Magnesia-based cements: a journey of 150 years, and cements for the future? Chem. Rev. 116 (2016) 4170–4204, https://doi.org/10.1021/acs.chemrev.5b00463.

[10] F. Winnefeld, E. Epifania, F. Montagnaro, E.M. Gartner, Further studies of the hydration of MgO-hydromagnesite blends, Cem. Concr. Res. 126 (2019), 105912, https://doi.org/10.1016/j.cemconres.2019.105912.

[11] M. Maryška, J. Blaha, K. Nemecek, Kinetics of hydration of magnesium oxide in aqueous suspension. Part 2 - the effect of conditions of firing basic magnesium carbonate on the specific surface area of magnesium oxide, in: Proceedings of Ceramics - Silikaty 41 (1), 1997, pp. 21–27.

[12] M. Maryška, J. Blaha, Hydration kinetics of magnesium oxide: part 3 - hydration rate of MgO in terms of temperature and time of its firing, Proceedings of Ceramics - Silikaty 41 (4) (1997) 121–123.

[13] V.S. Birchal, S.D.F. Rocha, M.B. Mansur, V.S.T. Ciminelli, A simplified mechanistic analysis of the hydration of magnesia, Can. J. Chem. Eng. 79 (2001) 507–511, https://doi.org/10.1002/cjce.5450790406.

[14] J.-L. Gálvez-Martos, R. Chaliulina, E. Medina-Martos, A. Elhoweris, A. Hakki, J. Mwanda, Y. Al-Horr, Eco-efficiency of a novel construction material produced by carbon capture and utilization, J. CO_2 Util. 49 (2021), 101545, https://doi.org/10.1016/j.jcou.2021.101545.

[15] A. Scott, C. Oze, V. Shah, N. Yang, B. Shanks, C. Cheeseman, A. Marshall, M. Watson, Transformation of abundant magnesium silicate minerals for enhanced CO_2 sequestration, Commun. Earth Environ. 2 (2021) 1–6, https://doi.org/10.1038/s43247-021-00099-6.

[16] S. Madeddu, M. Priestnall, E. Godoy, R.V. Kumar, S. Raymahasay, M. Evans, R. Wang, S. Manenye, H. Kinoshita, Extraction of $Mg(OH)_2$ from Mg silicate minerals with NaOH assisted with H_2O: implications for CO_2 capture from exhaust flue gas, Faraday Discuss. 183 (2015) 369–387, https://doi.org/10.1039/C5FD00047E.

[17] E. Nduagu, T. Björklöf, J. Fagerlund, J. Wärnå, H. Geerlings, R. Zevenhoven, Production of magnesium hydroxide from magnesium silicate for the purpose of CO_2 mineralisation – part 1: application to Finnish serpentinite, Miner. Eng. 30 (2012) 75–86, https://doi.org/10.1016/j.mineng.2011.12.004.

[18] N.T. Dung, R. Hay, A. Lesimple, K. Celik, C. Unluer, Influence of CO_2 concentration on the performance of MgO cement mixes, Cem. Concr. Compos. 115 (2021), 103826, https://doi.org/10.1016/j.cemconcomp.2020.103826.

[19] M.E. Aphane, E.M. van der Merwe, C.A. Strydom, Influence of hydration time on the hydration of MgO in water and in a magnesium acetate solution, J. Therm. Anal. Calorim. 96 (2009) 987–992, https://doi.org/10.1007/s10973-008-9095-y.

[20] O. Fruhwirth, G.W. Herzog, I. Hollerer, A. Rachetti, Dissolution and hydration kinetics of MgO, Surf. Technol. 24 (1985) 301–317, https://doi.org/10.1016/0376-4583(85)90080-9.

[21] S.D. Rocha, M.B. Mansur, V.S. Ciminelli, Kinetics and mechanistic analysis of caustic magnesia hydration, J. Chem. Technol. Biotechnol. 79 (2004) 816–821, https://doi.org/10.1002/jctb.1038.

[22] N.T. Dung, C. Unluer, Development of MgO concrete with enhanced hydration and carbonation mechanisms, Cem. Concr. Res. 103 (2018) 160–169, https://doi.org/10.1016/j.cemconres.2017.10.011.

[23] N.T. Dung, C. Unluer, Performance of reactive MgO concrete under increased CO_2 dissolution, Cem. Concr. Res. 118 (2019) 92–101, https://doi.org/10.1016/j.cemconres.2019.02.007.

[24] D. Filippou, N. Katiforis, N. Papassiopi, K. Adam, On the kinetics of magnesia hydration in magnesium acetate solutions, J. Chem. Technol. Biotechnol. 74 (1999) 322–328, https://doi.org/10.1002/(SICI)1097-4660(199904)74:4<322::AID-JCTB35>3.0.CO;2-L.

[25] E.M. van der Merwe, C. Strydom, A. Botha, Hydration of medium reactive industrial magnesium oxide with magnesium acetate, J. Therm. Anal. Calorim. 77 (2004) 49–56, https://doi.org/10.1023/B:JTAN.0000033187.61971.1d.

[26] X. Tang, Y. Ji, Y. Nie, L. Guo, Q. Liu, J. Zhao, T. Li, Y. Zhu, Three-phase hydration of magnesium oxide using hydration agents, Cryst. Res. Technol. 52 (2017) 1600393, https://doi.org/10.1002/crat.201600393.

[27] N.T. Dung, C. Unluer, Carbonated MgO concrete with improved performance: the influence of temperature and hydration agent on hydration, carbonation and strength gain, Cem. Concr. Compos. 82 (2017) 152–164, https://doi.org/10.1016/j.cemconcomp.2017.06.006.

[28] N.T. Dung, C. Unluer, Sequestration of CO_2 in reactive MgO cement-based mixes with enhanced hydration mechanisms, Construct. Build Mater. 143 (2017) 71–82, https://doi.org/10.1016/j.conbuildmat.2017.03.038.

[29] C. Unluer, A. Al-Tabbaa, Impact of hydrated magnesium carbonate additives on the carbonation of reactive MgO cements, Cem. Concr. Res. 54 (2013) 87–97, https://doi.org/10.1016/j.cemconres.2013.08.009.

[30] J. Zhang, G.W. Scherer, Comparison of methods for arresting hydration of cement, Cem. Concr. Res. 41 (2011) 1024–1036, https://doi.org/10.1016/j.cemconres.2011.06.003.

[31] N.C. Collier, J.H. Sharp, N.B. Milestone, J. Hill, I.H. Godfrey, The influence of water removal techniques on the composition and microstructure of hardened cement pastes, Cem. Concr. Res. 38 (2008) 737–744, https://doi.org/10.1016/j.cemconres.2008.02.012.

[32] E. Kordes, J. Petzoldt, Beitrag zur Aufklärung der Mischkristallbildung im quaternären System Li_2O-MgO-Cr_2O_3-Fe_2O_3, Z. Für Anorg. Allg. Chem. 335 (1965) 138–155, https://doi.org/10.1002/zaac.19653350304.

[33] A.A. Zhukhlistov, A.S. Avilov, D. Ferraris, B.B. Zvyagin, V.P. Plotnikov, Statistical distribution of hydrogen over three positions in the brucite $Mg(OH)_2$ structure from electron diffractometry data, Crystallogr. Rep. 42 (1997) 774–777, https://doi.org/10.1134/1.170692.

[34] G. Giester, C.L. Lengauer, B. Rieck, The crystal structure of nesquehonite, $MgCO_3 \cdot 3H_2O$, from Lavrion, Greece, Mineral. Petrol. 70 (2000) 153–163, https://doi.org/10.1007/s007100070001.

[35] R.R. Reeber, Lattice parameters of ZnO from 4.2° to 296°K, J. Appl. Phys. 41 (1970) 5063–5066, https://doi.org/10.1063/1.1658600.
[36] B. Lothenbach, P. Durdziński, K. De Weerdt, in: K. Scrivener, R. Snellings, B. Lothenbach (Eds.), Thermogravimetric Analysis, CRC Press, 2016, https://doi.org/10.1201/b19074.
[37] C. Kuenzel, F. Zhang, V. Ferrándiz-Mas, C.R. Cheeseman, E.M. Gartner, The mechanism of hydration of MgO-hydromagnesite blends, Cem. Concr. Res. 103 (2018) 123–129, https://doi.org/10.1016/j.cemconres.2017.10.003.
[38] G. Bassioni, R. Farid, M. Mohamed, R.M. Hammouda, F.E. Kühn, Effect of different parameters on caustic magnesia hydration and magnesium hydroxide rheology: a review, Mater. Adv. 2 (2021) 6519–6531, https://doi.org/10.1039/D0MA00887G.
[39] K. Nahdi, F. Rouquerol, M. Trabelsi Ayadi, $Mg(OH)_2$ dehydroxylation: a kinetic study by controlled rate thermal analysis (CRTA), Solid State Sci. 11 (2009) 1028–1034, https://doi.org/10.1016/j.solidstatesciences.2009.02.013.
[40] H. Nguyen, H. Santos, H. Sreenivasan, W. Kunther, V. Carvelli, M. Illikainen, P. Kinnunen, On the carbonation of brucite: effects of Mg-acetate on the precipitation of hydrated magnesium carbonates in aqueous environment, Cem. Concr. Res. 153 (2022), 106696, https://doi.org/10.1016/j.cemconres.2021.106696.
[41] S. Niu, K. Han, C. Lu, R. Sun, Thermogravimetric analysis of the relationship among calcium magnesium acetate, calcium acetate and magnesium acetate, Appl. Energy 87 (2010) 2237–2242, https://doi.org/10.1016/j.apenergy.2010.01.007.
[42] J.I. Langford, A.J.C. Wilson, Scherrer after sixty years: a survey and some new results in the determination of crystallite size, J. Appl. Cryst. 11 (1978) 102–113, https://doi.org/10.1107/S0021889878012844.
[43] A. Monshi, M.R. Foroughi, M.R. Monshi, Modified Scherrer equation to estimate more accurately nano-crystallite size using XRD, World J. Nano Sci. Eng. 2 (2012) 154–160, https://doi.org/10.4236/wjnse.2012.23020.
[44] P.J. Davies, B. Bubela, The transformation of nesquehonite into hydromagnesite, Chem. Geol. 12 (1973) 289–300, https://doi.org/10.1016/0009-2541(73)90006-5.
[45] G.L. Smithson, N.N. Bakhshi, Kinetics and mechanism of carbonation of magnesium oxide slurries, Ind. Eng. Chem. Process. Des. Dev. 12 (1973) 99–106, https://doi.org/10.1021/i260045a019.
[46] J.J. Thomas, S. Musso, I. Prestini, Kinetics and activation energy of magnesium oxide hydration, J. Am. Ceram. Soc. 97 (2014) 275–282, https://doi.org/10.1111/jace.12661.
[47] G.L. Smithson, N.N. Bakhshi, The kinetics and mechanism of the hydration of magnesium oxide in a batch reactor, Can. J. Chem. Eng. 47 (1969) 508–513, https://doi.org/10.1002/cjce.5450470602.
[48] J.J. Thomas, The instantaneous apparent activation energy of cement hydration measured using a novel calorimetry-based method, J. Am. Ceram. Soc. 95 (2012) 3291–3296, https://doi.org/10.1111/j.1551-2916.2012.05396.x.
[49] K. Eusterhues, F.E. Wagner, W. Häusler, M. Hanzlik, H. Knicker, K.U. Totsche, I. Kögel-Knabner, U. Schwertmann, Characterization of Ferrihydrite-soil organic matter coprecipitates by X-ray diffraction and Mössbauer spectroscopy, Environ. Sci. Technol. 42 (2008) 7891–7897, https://doi.org/10.1021/es800881w.
[50] Z. Yan-Rong, K. Xiang-Ming, L. Zi-Chen, L. Zhen-Bao, Z. Qing, D. Bi-Qin, X. Feng, Influence of triethanolamine on the hydration product of portlandite in cement paste and the mechanism, Cem. Concr. Res. 87 (2016) 64–76, https://doi.org/10.1016/j.cemconres.2016.05.009.
[51] R. Ma, J. Liang, X. Liu, T. Sasaki, General insights into structural evolution of layered double hydroxide: underlying aspects in topochemical transformation from brucite to layered double hydroxide, J. Am. Chem. Soc. 134 (2012) 19915–19921, https://doi.org/10.1021/ja310246r.
[52] N. Iyi, K. Kurashima, T. Fujita, Orientation of an organic anion and second-staging structure in layered double-hydroxide intercalates, Chem. Mater. 14 (2002) 583–589, https://doi.org/10.1021/cm0105211.
[53] E. Bernard, W.J. Zucha, B. Lothenbach, U. Mäder, Stability of hydrotalcite (Mg-Al layered double hydroxide) in presence of different anions, Cem. Concr. Res. 152 (2022), 106674, https://doi.org/10.1016/j.cemconres.2021.106674.
[54] J. Scheck, J.K. Berg, M. Drechsler, A. Kempter, A.E.S.V. Driessche, H. Cölfen, D. Gebauer, M. Kellermeier, New insights into the nucleation of magnesium hydroxide and the influence of poly(acrylic acid) during the early stages of Mg $(OH)_2$ crystallisation, CrystEngComm 24 (2022) 7718–7726, https://doi.org/10.1039/D2CE00896C.
[55] M. Liska, A. Wilson, J. Bensted, Special Cements, Lea's Chemistry of Cement and Concrete, Elsevier, in, 2019, pp. 585–640, https://doi.org/10.1016/B978-0-08-100773-0.00013-7.
[56] F.L. Sayles, W.S. Fyfe, The crystallization of magnesite from aqueous solution, Geochim. Cosmochim. Acta 37 (1973) 87–99, https://doi.org/10.1016/0016-7037(73)90246-9.
[57] J. Hövelmann, C.V. Putnis, E. Ruiz-Agudo, H. Austrheim, Direct nanoscale observations of CO_2 sequestration during Brucite $[Mg(OH)_2]$ dissolution, Environ. Sci. Technol. 46 (2012) 5253–5260, https://doi.org/10.1021/es300403n.
[58] C.E. White, N.J. Henson, L.L. Daemen, M. Hartl, K. Page, Uncovering the true atomic structure of disordered materials: the structure of a hydrated amorphous magnesium carbonate ($MgCO_3{\cdot}3D_2O$), Chem. Mater. 26 (2014) 2693–2702, https://doi.org/10.1021/cm500470g.
[59] X. Zhang, A.S. Lea, A.M. Chaka, J.S. Loring, S.T. Mergelsberg, E. Nakouzi, O. Qafoku, J.J. De Yoreo, H.T. Schaef, K.M. Rosso, In situ imaging of amorphous intermediates during brucite carbonation in supercritical CO_2, Nat. Mater. 21 (2022) 345–351, https://doi.org/10.1038/s41563-021-01154-5.
[60] O.S. Pokrovsky, J. Schott, A. Castillo, Kinetics of brucite dissolution at 25°C in the presence of organic and inorganic ligands and divalent metals, Geochim. Cosmochim. Acta 69 (2005) 905–918, https://doi.org/10.1016/j.gca.2004.08.011.